Synthesis of 1,6/7-(NO 2) 2 -Perylenediimide and 1,6/7-(NH 2) 2 -Perylenediimide as Regioisomerically Pure Materials**

Adèle Gapin, Arthur David, Magali Allain, Dorian Masson, Thomas Ave, Laura Le Bras, Piétrick Hudhomme, Antoine Goujon, Olivier Alévêque

Chemistry–A European Journal
Research Article
doi.org/10.1002/chem.202300652
Chemistry Europe
European Chemical Societies Publishing
www.chemeurj.org

Synthesis of 1,6/7-$(NO_2)_2$-Perylenediimide and 1,6/7-$(NH_2)_2$-Perylenediimide as Regioisomerically Pure Materials**

Adèle Gapin[+],[a] Arthur H. G. David[+],[a] Magali Allain,[a] Dorian Masson,[a] Olivier Alévêque,[a] Thomas Ave,[a] Laura Le Bras,*[b] Piétrick Hudhomme,*[a] and Antoine Goujon*[a]

Abstract: The use of perylenediimide (PDI) building blocks in materials for organic electronic is of considerable interest. This popular n-type organic semiconductor is tuned by introducing peripheral groups in their *ortho* and *bay* positions. Such modifications radically alter their optoelectronic properties. In this article, we describe an efficient method to afford regioisomerically pure 1,6/7-$(NO_2)_2$- and $(NH_2)_2$-PDIs employing two key steps: the selective crystallization of 1,6-$(NO_2)_2$-perylene-3,4,9,10-tetracarboxy tetrabutylester and the nitration of regiopure 1,7-Br_2-PDI with silver nitrite. The optoelectronic properties of the resulting regioisomerically pure dinitro, diamino-PDIs and bisazacoronenediimides (BACDs) are reported and demonstrate the need to separate both regioisomers of such n-type organic semiconductors for their inclusion in advanced optoelectronic devices. For the first time, the two regioisomers of the same PDI starting material are available on the multigram scale, which will stimulate the exploration of regioisomerism/properties relationship for this family of dyes.

Introduction

Perylenediimide (PDI) based materials have been increasingly drawing attention in organic electronics.[1,2] Their high electron-affinity and strong visible-light absorption combined with the high electron-mobilities measured in thin films make them attractive n-type organic semiconductors.[3] They can be found in a variety of organic electronics devices as active materials such as Organic Solar Cells (OSCs) as Non-Fullerene-Acceptors (NFAs)[4,5] or Electron Transporting Layer[6,7] for example and they are rising in chiral optoelectronics applications.[8] The choice of imide side-chain usually controls their self-assembly and solubility,[9] while the modification of their *ortho* and *bay* positions drastically change their optical and electronic properties:[10,11] in consequence, an intense synthetic work has been made to introduce various chemical functionalities and extend/dope their aromatic core.[12–15] The most popular and widespread strategy to functionalize the *bay* position is to first perform an halogenation.[16–18] The brominated PDIs can be engaged in palladium-catalysed cross-coupling reactions or nucleophilic aromatic substitutions among others.[19] The use of a large excess of bromine allows for the preparation of Br_2-PDI, an essential starting material of conjugated polymers[20] or core-extended polyaromatic hydrocarbons diimides.[21] However, preparing this important intermediate of PDI chemistry results in a mixture of 1,6-Br_2-PDI and 1,7-Br_2-PDI regioisomers.[22] Jager and collaborators reported a strategy to prepare regioisomerically pure 1,7-Br_2-PDI starting from the preparation of perylene-3,4,9,10-tetracarboxy tetrabutylester (PTE).[23] After bromination, the 1,7 regioisomer can be separated and obtained pure on the multi-gram scale by successive crystallizations. 1,7-Br_2-PTE can then be converted into the desired 1,7-Br_2-PDI in two efficient steps. However, to our knowledge, there are no methods giving access to the pure 1,6-Br_2-PDI regioisomer. In consequence, the systematic study of the effect of regioisomery on the optoelectronic properties of materials prepared from these halogenated precursors remains out of reach since only one can be reliably prepared in a regiopure fashion. Noteworthy is the fact that, in very rare cases, the PDI regioisomers can be separated and isolated at a later stage after several synthetic steps,[24] but this method is not generalizable to all 1,6/7 PDI mixtures. Very recently, the groups of Wu and Xia reported how to prepare 1,6-$(OTf)_2$PDI starting from a tetrabrominated perylenemonoimide after four additional synthetic steps.[25] This route allows the preparation of a derivative of analogous reactivity to its halogenated counterpart, which can be engaged into Pd-catalysed cross-coupling reactions. However, it requires a significant synthetic work, including a Pd-catalysed imide formation involving the use of hazardous carbon monoxide.

[a] *Dr. A. Gapin,[+] Dr. A. H. G. David,[+] Dr. M. Allain, D. Masson, Dr. O. Alévêque, T. Ave, Prof. P. Hudhomme, Dr. A. Goujon*
Univ Angers, CNRS, MOLTECH-Anjou, SFR MATRIX
49000 Angers (France)
E-mail: pietrick.hudhomme@univ-angers.fr
antoine.goujon@univ-angers.fr

[b] *Dr. L. Le Bras*
Laboratoire Chrono-environnement (UMR 6249)
Université de Franche-Comté
16 route de Gray, 25030 Besançon (France)
E-mail: laura.le_bras@univ-fcomte.fr

[+] *These authors contributed equally to this work.*

[**] *A previous version of this manuscript has been deposited on a preprint server (https://chemrxiv.org/engage/chemrxiv/article-details/63c92ddef604-d148ec5bbbf8).*

Supporting information for this article is available on the WWW under https://doi.org/10.1002/chem.202300652

Nevertheless, this work and all effort directed toward the study of regiopure material is justified. PDI regioisomers have noticeably different optical and electronic properties, in addition to having different solid-state packing, which greatly affect their effective frontiers orbital energy levels and charge diffusion ability in thin films. These differences has been shown to greatly affect the performances and properties of organic electronic devices,[26,27] justifying the development of a synthetic strategy offering regiopure 1,6 and 1,7 precursors of the same material on large scale.

Recently, mono- and dinitrated PDIs (NO_2-PDIs and $(NO_2)_2$-PDIs) have demonstrated their potential as an alternative to brominated PDI analogs: they are prepared faster, in higher yield and selectivity and require little purification effort.[28] Moreover, reactivity-wise, NO_2-PDIs appear more versatile than their halogenated equivalents. Not only they can be engaged in nucleophilic aromatic substitutions, hetero-annulation reactions with atoms such as oxygen, sulfur, selenium and nitrogen, and their use as electrophile in Pd-catalysed cross-coupling reactions has been recently demonstrated.[29–31] Moreover, they can be reduced into NH_2-PDI, a material precursor of AzaBenzannulated PDIs and BisAzaCoroneneDiimides (BACDs), when using $(NH_2)_2$-PDI)[32–34] which both recently showed promising results as organic n-type semiconductors,[35,36] fluorescent probes[37] and NFAs in OSCs.[38] Therefore, the development of synthetic pathways to efficiently prepare regioisomerically pure 1,6/7-$(NO_2)_2$-PDIs and 1,6/7-$(NH_2)_2$-PDIs is more relevant than ever. Studies report the use of pure 1,7-$(NO_2)_2$-PDIs and 1,7-$(NH_2)_2$-PDIs regioisomers, stating that they were obtained by successive crystallizations.[36,37,39–41] However, the solvent used to do so has not been reported and the efficiency of this kind of purification is dependent on the nature of the imide chains used. Another work reports the use of pure 1,6/7-$(NO_2)_2$PDIs and their subsequent reduction.[42,43] The pure nitrated regioisomers were separated by high-performance liquid-chromatography, a technique limiting the scale of their preparation to a small amount of material and that is again dependent on the nature of the imide chains, limiting once again the exploration or regioisomery-dependent properties of complex materials requiring several additional synthetic steps Therefore, there is no efficient and scalable procedure to prepare grams of regiopure 1,6/7-$(NO_2)_2$-PDIs and 1,6/7-$(NH_2)_2$-PDIs to date.

Herein, we report a method that can afford for the first time both 1,6 and 1,7 pure regioisomers of $(NO_2)_2$-PDIs and $(NH_2)_2$-PDIs on multi-grams scale, to be further used as starting materials of n-type semiconductors (Figure 1). This investigation differs from previous works on brominated PDI where only 1,7-Br_2-PTE and 1,7-Br_2-PDI could be isolated. This method relies on the nitration or bromination of PTE. The key steps are the isolation of pure 1,6-$(NO_2)_2$-PTE by selective crystallization confirmed by single crystal X-ray diffraction, and the efficient nitration of 1,7-Br_2-PDI by treatment with silver nitrite.

Results and Discussion

Synthesis of regiopure 1,6-$(NO_2)_2$-PDI and 1,7-$(NO_2)_2$-PDI

PTE **1** was prepared and nitrated following procedures from the literature[44] to afford a 55:45 mixture of 1,6/7-$(NO_2)_2$-PTE **2** (Figure 2a). We attempted to apply the same crystallisation conditions in a mixture CH_2Cl_2/CH_3CN that are reported to separate 1,7-Br_2-PTE from 1,6-Br_2-PTE.[23] Large needle-like orange crystals were formed and recovered by filtration. After a second crystallization, ^{1}H NMR spectrum confirmed that a single regioisomer was isolated (Figure 2b). The same results were obtained by performing two successive recrystallizations in hot CH_3CN. The filtered crystals were suitable for X-ray diffraction, and their study allowed us to unambiguously determine that the isolated regioisomer was 1,6-$(NO_2)_2$-PTE **1,6-2** (Figure 2c, Figure S64). The compound crystallizes in triclinic *P*-1 space group. The structure presents a twisted angle of 17.8° between the two naphthalene fragment of the perylene core, comparable to those observed for PDI analogues.[30] The molecules are

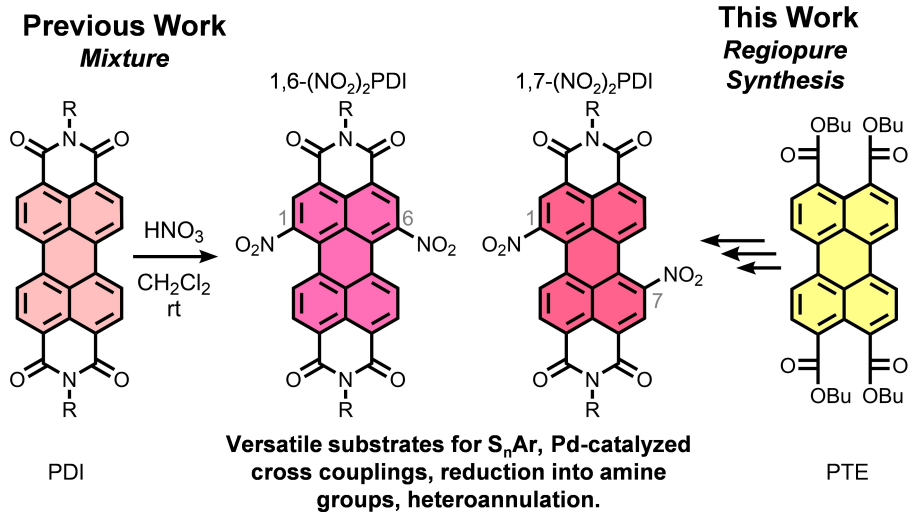

Figure 1. Conventional non-regioselective preparation of 1,6/7-$(NO_2)_2$-PDIs by treatment with fuming nitric acid and the regiopure pathway starting from PTE.

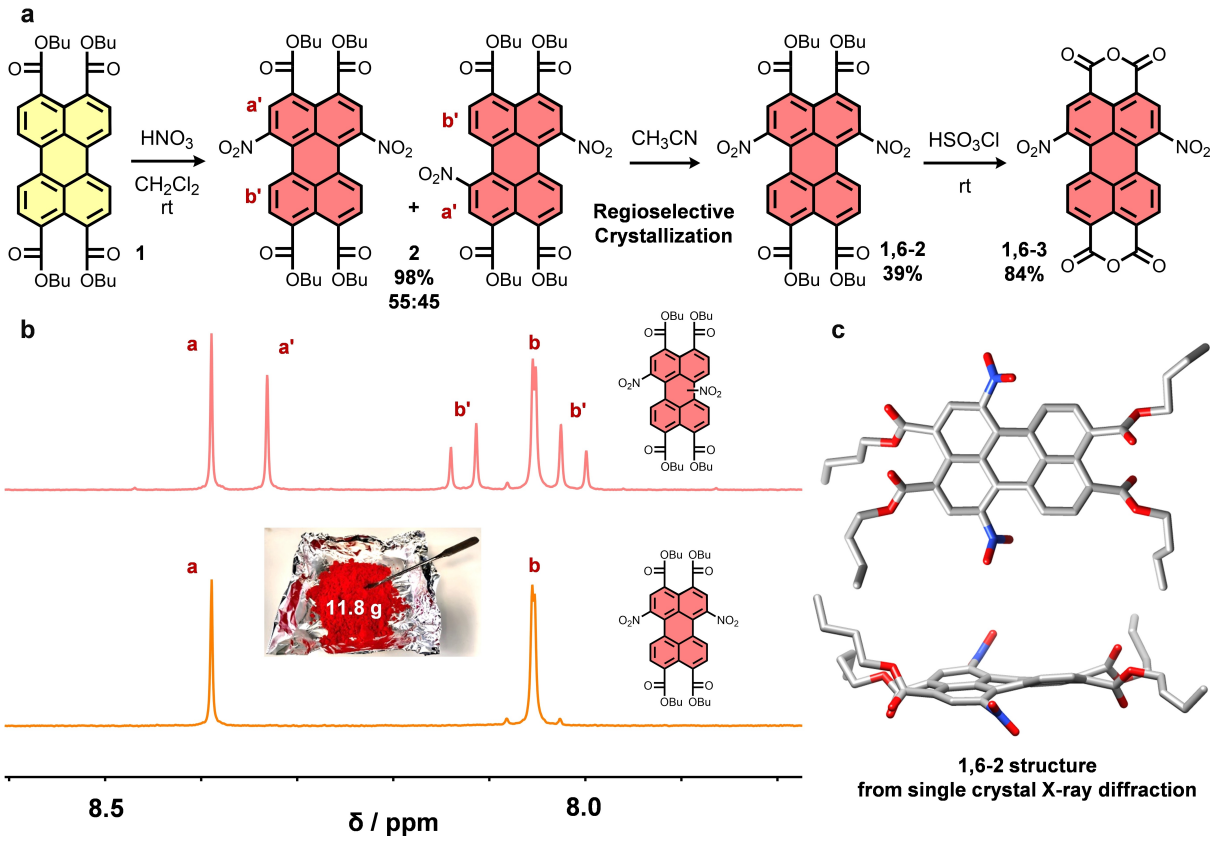

Figure 2. a) Synthesis of regioisomerically pure 1,6-$(NO_2)_2$-PTCDA **1,6-3**. b) Partial ^{1}H NMR spectra in $CDCl_3$ (300 MHz) of the 55:45 mixture of 1,6/7-$(NO_2)_2$-PTE **2** (top) and pure 1,6-$(NO_2)_2$-PTE **1,6-2** (bottom) obtained after two crystallizations. c) Molecular structure of 1,6-$(NO_2)_2$-PTE **1,6-2** obtained by single-crystal X-ray diffraction, from above and from the side, hydrogen atoms and solvent molecules omitted for clarity.

stacked in a head to tail manner along the *a* axis of the unit cell with a distance of 3.53 Å and 3.56 Å between them (see Figure S65). Deposition Number 2226011 (for 1,6-2) contains the supplementary crystallographic data for this paper. These data are provided free of charge by the joint Cambridge Crystallographic Data Centre and Fachinformationszentrum Karlsruhe Access Structures service. The regioisomer obtained by successive precipitations of $(NO_2)_2$-PTE here is the opposite one as in the case of Br_2-PTE. It was obtained in a 39% yield compared to the initial mixture **2** containing 55% of **1,6-2**, which gives a 71% yield for the two recrystallizations. We attempted this crystallization in other solvents to isolate the 1,7-$(NO_2)_2$-PTE regioisomer via a similar strategy, in particular in THF, toluene, acetone, pentane, dichloromethane and diethyl ether. Unfortunately, the selective crystallization of 1,7-$(NO_2)_2$-PTE was never observed: in all cases the proportion of 1,6-$(NO_2)_2$-PTE **1,6-2** increased in the solid recovered after filtration. The dye **1,6-2** was further efficiently transformed into 1,6-$(NO_2)_2$-perylenetetracarboxylic-dianhydride or 1,6-$(NO_2)_2$-PTCDA **1,6-3** by a reaction with chlorosulfonic acid. This key intermediate can be reacted with any amine of choice to afford regiopure 1,6-$(NO_2)_2$-PDIs **1,6-4** (Figure 3a) following a simple four steps sequence, starting from materials that can be prepared on tenth of gram scale in the laboratory following well-known procedures.

With one pure regioisomer in hand, we investigated how to convert 1,7-Br_2-PTE into its nitrated equivalent 1,7-$(NO_2)_2$-PTE equivalent. We prepared 1,7-Br_2-PTE by following the method reported by Jager and collaborators.[23] Several reports describe how to substitute bromine by nitro groups via copper-catalysed reactions involving nitrite salts.[45–47] However, such reaction led to the decomposition of 1,7-Br_2-PTE, as it yielded a black insoluble material that could not be characterized. The replacement of a bromine atom by a nitro group was reported on thiophene derivatives by the simple use of silver nitrate.[48] 1,7-Br_2-PTE was refluxed in toluene in presence of an excess of $AgNO_3$ which led to its very slow conversion into a mixture of mono nitrated species and decomposition products along with a small amount of targeted material. $AgNO_3$ was replaced by $AgNO_2$ hoping that silver nitrite could lead to the target by S_NAr-type reaction. 1,7-Br_2-PTE was refluxed in toluene in presence an excess of $AgNO_2$ and this time the targeted species 1,7-$(NO_2)_2$-PTE was a formed along the mononitrated derivative and a significant amount of remaining starting material. These encouraging results suggested that the reaction should perform better on the more reactive and electron-deficient 1,7-Br_2-PDI **1,7-6**. Therefore, 1,7-Br_2-PTCDA **1,7-5** was prepared and reacted with an amine to form 1,7-Br_2-PDI **1,7-6**. This intermediate was reacted with $AgNO_2$ in toluene at reflux temperature in a pressured vial, which afforded the regiopure 1,7-$(NO_2)_2$-PDI **1,7-**

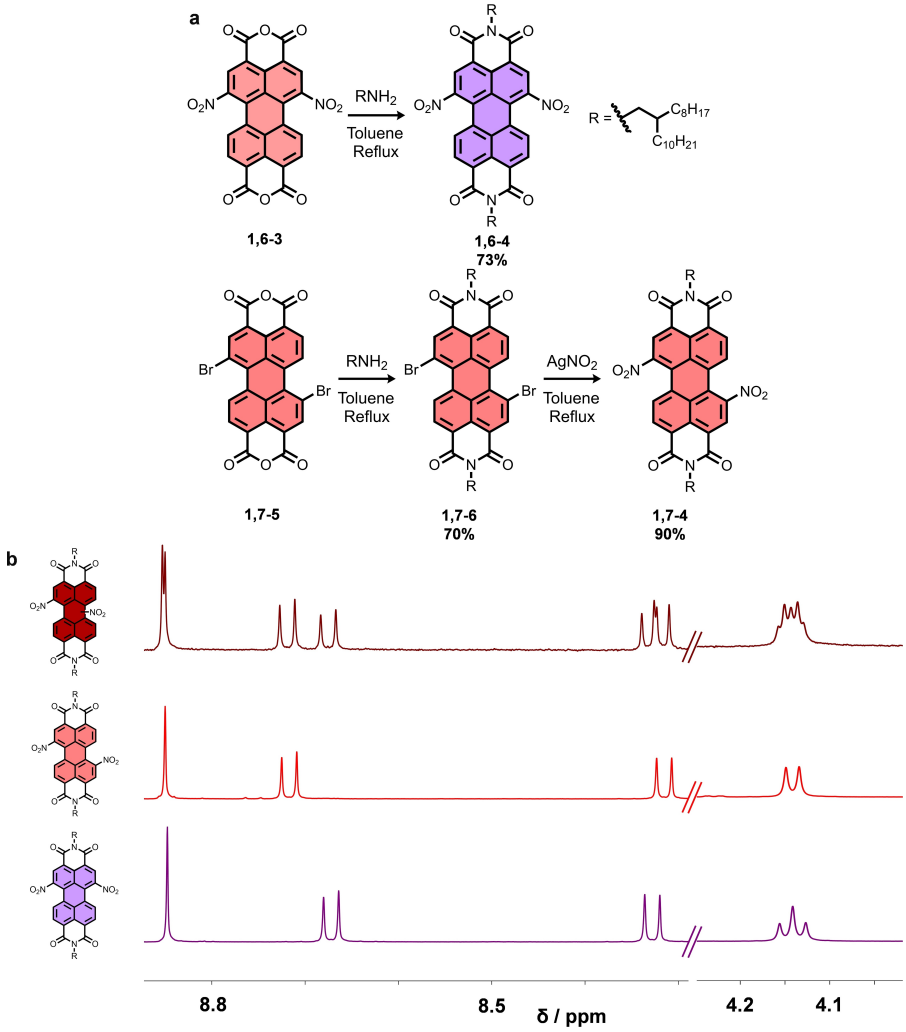

Figure 3. a) Synthesis of regioisomerically pure 1,7-$(NO_2)_2$-PDI **1,7-4** and 1,6-$(NO_2)_2$-PDI **1,6-4**. b) Partial ^{1}H NMR spectra in $CDCl_3$ (500 MHz) of the 1 : 1 mixture of 1,6/7-$(NO_2)_2$-PDI **4** (top), pure 1,6-$(NO_2)_2$-PDI **1,6-4** (middle) and pure 1,7-$(NO_2)_2$-PDI **1,7-4** (bottom).

4 in an excellent 90 % yield (Figure 3a). Adjusting and lowering the amount of silver nitrite afforded the mono-substituted compound 1-(Br)-7-(NO_2)-PDI **S1**, which could be an interesting intermediate for the preparation of dissymmetrical compounds (see Supporting Information, Scheme S3). ^{1}H NMR spectra comparison of **1,6-4, 1,7-4**, and the mixture of regioisomers resulting from the direct nitration of a PDI bearing the same imide chains (see Supporting Information, Scheme S5) confirms that we developed an efficient synthetic pathway to prepare regiopure 1,6-$(NO_2)_2$-PDI **1,6-4** and 1,7-$(NO_2)_2$-PDI **1,7-4**. It should be noted that our synthesis of $(NO_2)_2$-PDI as mixture of regioisomers affords an approximately 1 : 1 ratio.[30] as opposed to other reports in the literature.[34]

We further reduced the nitro groups into corresponding amines to obtain pure 1,6-$(NH_2)_2$-PDI **1,6-7** and 1,7-$(NH_2)_2$-PDI **1,7-7** by reaction with hydrazine monohydrate in presence of Pd/C (Figure 4). The comparison of their ^{1}H NMR spectra to the regioisomeric mixture can be seen in Figure S52 and confirms that there was no regioisomerisation during this process. These dyes were further converted into BACD derivatives following a light-driven procedure recently reported by our group,[49] which afforded the regiopure extended imide materials **1,6-8** and **1,7-8** in high yields (Figure 4). Again, no regioisomerisation was observed (Figure S53). Analogous materials prepared from other aldehydes were reported as single 1,6/7 regioisomers before but at the cost on multiple tedious column chromatography performed on the mixture.[32]

Striking visual differences could be observed for dried samples of **1,6-4** and **1,7-4**. The 1,6 derivative displays a deep purple colour while the 1,7 one shows a vibrant red tone. Similarly, different shades of blue can be seen for the 1,6/7-$(NH_2)_2$-PDI regioisomers **1,6-7** and **1,7-7**. At last, the two BACD derivatives **1,6-8** and **1,7-8** also display variations of orange colour.

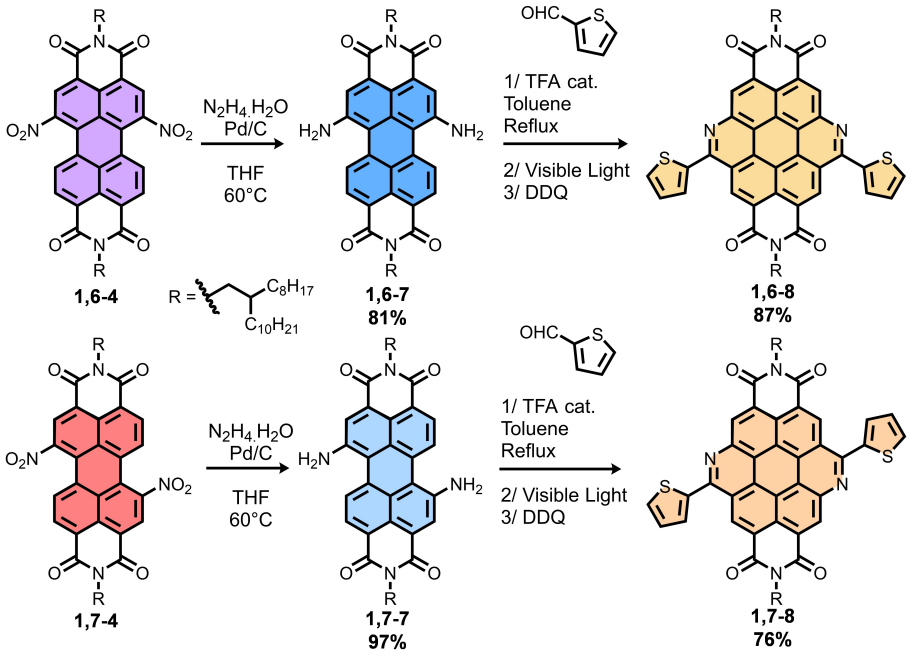

Figure 4. Synthesis of regioisomerically pure 1,6-$(NH_2)_2$-PDI **1,6-7** and 1,7-$(NH_2)_2$-PDI **1,7-7** and corresponding BisAzaCoroneneDiimides **1,6-8** and **1,7-8**.

Regioisomerism-dependant optoelectronic properties

UV-visible spectroscopy measurements were performed to compare the photophysical properties of the regioisomers (Figure 5). The dinitro derivative **1,6-4** shows a slightly red-shifted (520 nm) absorption maximum and a small shoulder at low energy compared to the **1,7-4** regioisomer (518 nm) as displayed in Figure 5a. In film, both regioisomers see their absorption maximum red-shifting and a narrower band at low energy (Figure S4 and S8). Amine-functionalized derivatives also exhibit differences in absorption maximum: 587 nm for **1,6-7** and 616 nm for **1,7-7** (Figure 5b). Once again, the films lead to a red-shift of the absorption maximum in both cases (Figure S12 and S16), but in the case of the 1,6 regioisomer, an inversion of the absorption ratio between the first and second shoulders of the first absorption band can be observed (Figure S12). At last, the thiophene-appended BACD derivatives absorbs light up to around 550 nm but they display a maximum at higher energy: at 389 nm for **1,6-8** and 373 nm for **1,7-8** (Figure 5c). Their processing in films red-shifts their absorption up to around 600 nm (Figure S20 and S24) along with a noticeable loss of fine structure more pronounced for the 1,6 regioisomer than the 1,7 one. All the compounds showed high extinction molar coefficient (ε) in solution, with little differences depending on the regioisomers when it comes to the nitrated or amino derivatives. However, **1,6-8** absorbs light more strongly than **1,7-8** at high energy. These dyes are poorly fluorescent (quantum yields between 0 and 5%, see Table 1 and S1 and Figure 5a, b, c). Overall the differences of optical properties for each regioisomers of the same compound and the variations observed when going from solutions to films in term of band position and shape strongly suggest different solid-state organization. The optical properties of the films were not significantly affected by thermal annealing for nitro compounds **1,6-4** and **1,7-4** and BACD **1,6-8** and **1,7-8** (Figure S3, S7, S19, S23). In the case of the amines **1,6-7** and **1,7-7** (Figure S11, S15), a decrease in absorption accompanied by a slight blue shift of the maximum of absorption are observed which indicates a reorganisation of the chromophores upon annealing. Figure 5d illustrates these differences as seen with the naked eye.

Table 1. Summary of the optoelectronic properties of the regioisomerically pure dyes **4** and **7** in CH_2Cl_2 and **8** in $CHCl_3$.

Compound	λ_{abs} [nm][a]	ε [$M^{-1}cm^{-1}$][b]	λ_{em} [nm]	Φ_f [%]	E^{LUMO} [eV]	E^{HOMO}_{calc} [eV]	$\Delta E^{HOMO-LUMO}$ [eV]
1,6-4	520	4.0×10^4	576	0.062	−4.29	−6.37	2.08
1,7-4	518	4.0×10^4	572	1.1	−4.30	−6.47	2.17
1,6-7	587	2.7×10^4	696	N/A	−3.55	−5.17	1.62
1,7-7	616	2.8×10^4	678	N/A	−3.55	−5.13	1.58
1,6-8	389	5.9×10^4	532	4.9	−3.68	−5.75	2.07
1,7-8	373	4.4×10^4	541	4.0	−3.67	−5.74	2.07

[a] Maximum wavelength of the strongest energy absorption band given for the spectrum in solution. [b] Extinction coefficient of the strongest energy absorption band.

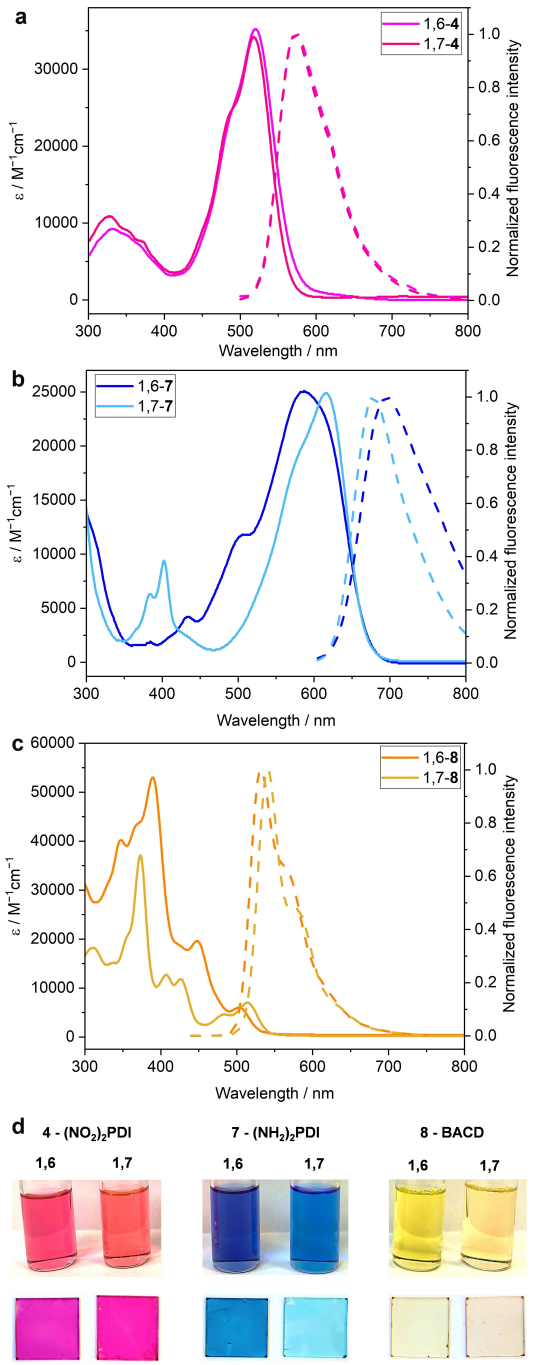

Figure 5. Absorption (solid line) and normalized emission (dashed lines) spectra of the regioisomerically pure dyes **4** (**a**, λ_{exc} = 480 nm), **7** (**b**, λ_{exc} = 586 nm) recorded in CH_2Cl_2 and **8** (**c**, λ_{exc} = 387 nm) recorded in $CHCl_3$ at a concentration of *ca.* 1×10^{-5} M. **d**) Photograph of solution of the regioisomerically pure compounds **4**, **7** and **8** (top) and corresponding spin-coated thin films on glass substrates (bottom).

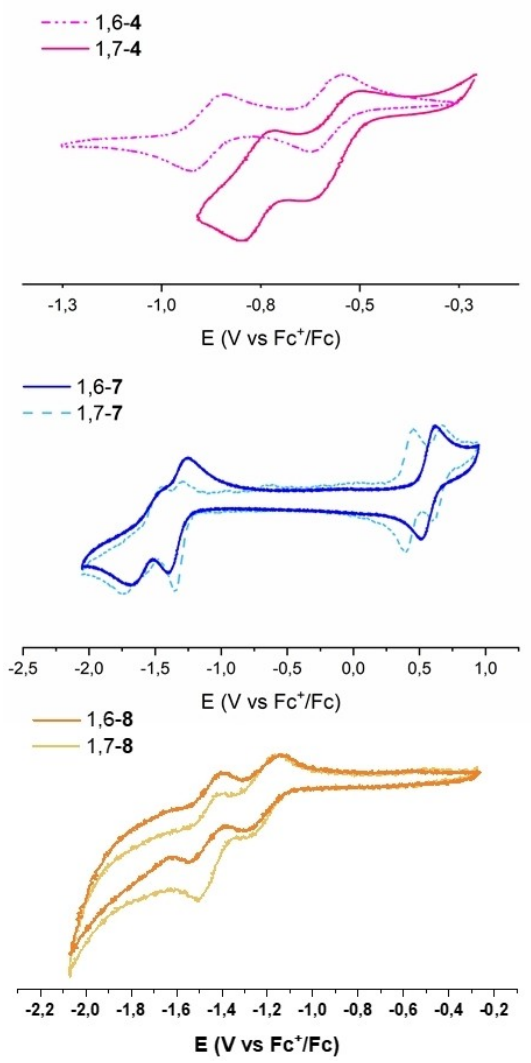

Figure 6. Cyclic voltammetry of dyes **4**, **7** (in CH_2Cl_2), and **8** (in $CHCl_3$), scanned toward negative potentials, with *n*-Bu_4NPF_6 (0.1 M) as electrolyte.

These studies were complemented by cyclic voltammetry, performed in a glovebox in CH_2Cl_2 (for **4** and **7**) and $CHCl_3$ (for **8**) with 0.1 M *n*-Bu_4NPF_6 (Figure 6). When scanning toward negative potentials, **1,6-4** and **1,7-4** reveals the expected two reduction waves typical of PDI dyes. The 1,6 regioisomer can be reduced at a higher potential compared to the 1,7 regioisomer, making it a better electron acceptor. The amine-decorated compounds **1,6-7** and **1,7-7** show the same two reduction waves but can also be oxidized when scanning toward positive potentials. Two oxidation waves can be detected for **1,7-7** in the range studied, whereas only one for the **1,6-7** analogue. If both compounds can be reduced at similar potential, the **1,7-7** regioisomers is oxidized at a lower potential. When it comes to BACD derivatives, the first reduction is observed at −1.23 V for **1,6-8** and −1.14 V for **1,7-8** (vs Fc^+/Fc) and the resulting HOMO and LUMO energy levels are analogous. Nevertheless, similarly to the case of the spectroscopic studies, the electrochemical investigations presented here highlight the differences of electronic behaviour and properties of each distinct regioisomer. It is worth emphasizing that the optoelectronic properties of chromophores, including semiconductors, are tuned on account of their regioisomerism.[50–54] The different optoelectronic properties of the regioisomerically pure dyes are summarized in Table 1, which demonstrates and renders the separation of

these regioisomers of key importance for their implementation in advanced optoelectronic devices.

DFT calculations

To gain deeper insights into the photophysical behaviour of the different regioisomers, ground state optical properties were computed using density functional theory (DFT) and its time-dependent component (TD-DFT). The CAM-B3LYP/6-31 + G(d) level of theory was used along with an implicit solvation model, either chloroform or dichloromethane depending on the considered compound. This protocol has already been used previously on similar molecules.[55–57] Further details about the computational approach are provided in the Supporting Information.

After an optimization step, the optical properties, and especially the main absorption peak (λ_{abs} and λ_{calc}), of the two regioisomers of **4**, **7**, and **8** were computed and compared to the experimental ones (Table 2). The difference between the calculated and the experimental λ are systematically lower than the traditional accuracy threshold of 0.2 eV, indicating an adequate computational approach. Beyond the reproduction of the main absorption peak for each regioisomer, it has also been possible to retrieve quantitatively the difference between regioisomers (red-shift for **1,7-7** compared to **1,6-7**, blue-shift for **1,7-8** compared to **1,6-8** and no significant modification between **1,6-4** and **1,7-4**) and to reproduce nicely the shape of the different spectra (Figure S29).

For **4** and **7** the main absorption peak corresponds to a $S_0 \rightarrow S_1$ excitation and is described by HOMO–LUMO transition (Table 2 and Figure 7). For **8**, the main absorption peak ascribes to a $S_0 \rightarrow S_3$ excitation, mainly described by HOMO–LUMO + 1 (**1,6-8**) and HOMO-2-LUMO (**1,7-8**) transitions and by HOMO–LUMO transitions in a lesser extent for both molecules (Figure S28). All the orbitals that are involved are localized on the conjugated core of the molecules, corresponding to π–π* transitions, reinforcing the choice of not considering the alkyl lateral chains (Table S**2**). The charge transfer (CT) character was also investigated. Due to the symmetry of the molecules, especially the 1,7 regioisomers, all the descriptors (d_{CT}, q_{CT} and $||\vec{\mu}_{CT}||$) have low values. It is due to the fact that the transitions are localized only on the perylene core. The representation of the transition electronic density variation (Figure S30) and of $\vec{\mu}_{CT}$ (Figure S31) are gathered in the Supporting Information. It is worth noticing that the *bay*-substituents are involved, at variable levels, in the main absorption band and can, thus, be tuned to modify the absorption spectra of the molecules. For

Table 2. Experimental (λ_{abs}, nm) and calculated (λ_{calc}, nm) absorption maxima for each regioisomer of **4**, **7**, and **8**. The absolute energy difference between experimental and calculated λ ($|\Delta E|$, in eV), the attribution and the description of the transition, the corresponding oscillator strength (*f*), the charge-transfer distance (d_{CT}, in Å), amount of transferred electron (q_{CT}, in |e|), and the norm of transition dipole moment, ($||\vec{\mu}_{CT}||$, in D), have also been reported for each transition.

Compound	λ_{abs}	λ_{calc}	$\lvert\Delta E\rvert$	Attribution	Description	*f*	d_{CT}	q_{CT}	$\lvert\lvert\vec{\mu}_{CT}\rvert\rvert$
1,6-4	520	522	0.01	$S_0 \rightarrow S_1$	H→L	0.90	0.71	0.40	1.36
1,7-4	518	524	0.03	$S_0 \rightarrow S_1$	H→L	0.86	0.18	0.39	0.35
1,6-7	587	553	0.13	$S_0 \rightarrow S_1$	H→L	0.90	0.72	0.47	1.60
1,7-7	616	577	0.14	$S_0 \rightarrow S_1$	H→L	0.85	0.30	0.46	0.66
1,6-8	389	394	0.04	$S_0 \rightarrow S_3$	H→L + 1	2.58	0.21	0.54	0.54
1,7-8	373	374	0.01	$S_0 \rightarrow S_3$	H-2→L	2.36	0.12	0.54	0.31

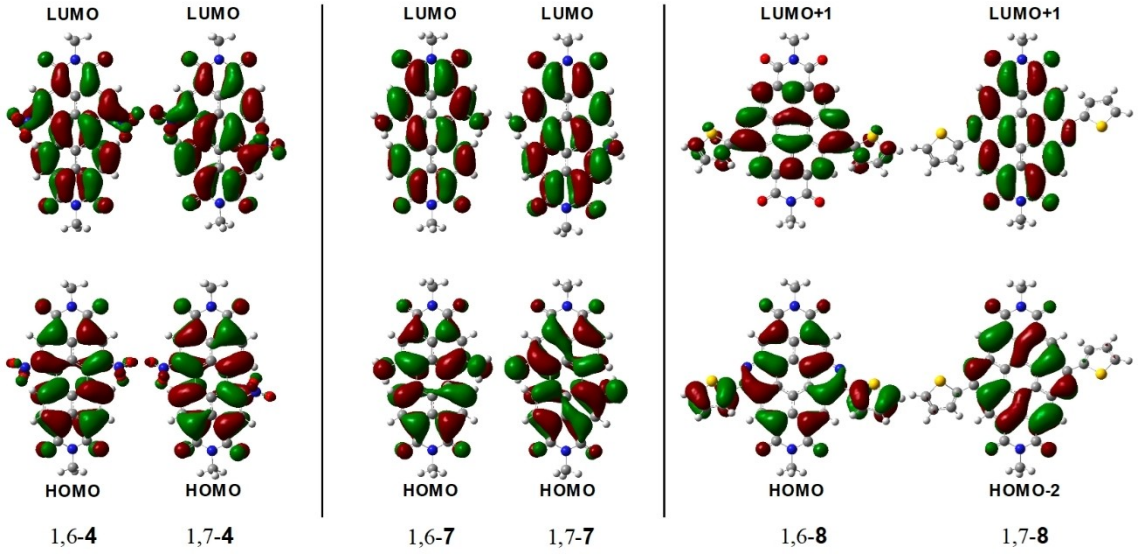

Figure 7. Representation of the most important molecular orbitals corresponding to λ_{calc} for each regioisomer of **4**, **7** and **8**. Isodensity = 0.0004 a.u.

example, going from nitro (**4**) to amino (**7**) groups leads to a red-shift of the main absorption band, theoretically and experimentally. This bathochromic shift can be explained by looking at the orbitals involved in the transition. In the case of compound **7**, the amino substituents are involved in the π system while this is less the case for compound **4** (Figure 7). The π system of **7** is, thus, more extended than that of **4**. Since the absorption bands are shifted, the resulting colour of the solutions are different. Compound **4** absorbs in the blue-to-green area and appears to be red in solution while compound **7** absorbs in the green to orange area and is blue in solution. In the case of compound **8**, the main absorption band does not always involve the thiophene substituents (Figure 7 and Figure S28) and it results in a less extended conjugated system with a lower λ_{abs}. The differences in terms of optoelectronic properties between 1,6 and 1,7 isomers for the three molecules in solution are, however, subtle and may be attributed to small differences induced by the symmetry (axial for 1,6 and centrosymmetry for 1,7) and illustrated through charge-transfer parameters (see d_{CT} and μ_{CT} in Table 2). Theoretical calculations can also help to understand the differences observed for the thin films. To understand the apparent differences between **1,6-4** (purple) and **1,7-4** (red) we have performed calculations considering dimers, to mimic the simplest assembly of molecules within a thin film. The geometry and structure of dimers was optimized by molecular mechanics, before the imide chains were replaced with methyl groups to simplify the calculation of the optical and electronic properties. When dimers of both regioisomers are considered, a systematic flattening of the molecules can be observed. The value of the dihedral angle between the two sides of the perylene core decreases from around 18 ° to 14 ° (Figure S32). This modification induces an increase of the conjugation of the molecules and thus a red-shift of the computed optoelectronic properties (Table S**3**), as observed experimentally (Figure S4 and Figure S8). Looking closely to the transitions, different behaviours are observed for compounds **1,6-4** and **1,7-4**. In the case of compound **1,6-4**, due to the structure of the molecule and its packing, the transition involves both molecules while the transition for compound **1,7-4** only involves one molecule at a time (Figure S33). **1,6-4** acts as a real dimer, increasing the area of the π system whereas **1,7-4** acts as two close but independent molecules. Depending on the considered regioisomer, the packing will be different as well as the corresponding optoelectronic properties and the resulting apparent colour of the thin film.

Conclusion

We have developed here an efficient regioselective synthetic strategy to prepare 1,6/7-$(NO_2)_2$-PDI and 1,6/7-$(NH_2)_2$-PDI. These derivatives can be engaged into similar reactions as their halogenated equivalents such as S_NAr, Pd-catalysed couplings, hetero-annulations, reductions and more. More importantly, they also represent the first example of bis-*bay*-substituted PDIs starting materials available as both pure 1,6 and 1,7 regioisomers on multi-grams scale, in opposition to brominated starting materials previously isolated only as their 1,7 regioisomer. The well-noticeable differences in optical and electronic properties measured here for each regioisomer highlight the importance of this new route, as they should afford different performances and characteristics in devices. This combination of unique advantages makes these nitro and amino derivatives highly attracting building-blocks for the development of new n-type materials for organic electronics.

Experimental Section

Materials and general methods: Thin Layer Chromatography (TLC) was conducted on pre-coated aluminium sheets with 0.20 mm MerckAlugram SIL G/UV254 with fluorescent indicator UV254. Column chromatography was carried out using Sigma-Aldrich silica gel 60 (particle size 63–200 μm). UV-Vis absorptions were recorded on a Shimadzu UV-1800 UV-Vis spectrophotometer using quartz cell (pathlength of 1 cm). Fluorescence was measured on a Shimadzu RF-6000 Spectrophotometer using quartz cell (pathlength of 1 cm). Quantum yields were measured on a Jasco FP-8500 Spectrophotometer equipped with an ILF-835 integration sphere. Cyclic voltammetry experiments were carried out at room temperature under Argon in a glovebox with a Bio-Logic SAS SP-150 potentiostat. Photoreactions were performed on an easy-Photochem flow photoreactor from Vapourtec equipped with a photochemical reactor UV-150 equipped with white LEDs. Nuclear magnetic resonance (NMR) ^{1}H and ^{13}C spectra were obtained on a Bruker 300 MHz Avance III spectrometer (300 MHz for ^{1}H) or 500 MHz Advance III HD spectrometer (500 MHz for ^{1}H and 125 MHz for ^{13}C). Chemical shifts were reported in ppm according to tetramethylsilane using the solvent residual signal as an internal reference ($CDCl_3$: $\delta_H = 7.26$ ppm, $\delta_C = 77.16$ ppm; D_2SO_4: $\delta_H = 11.20$ ppm). Coupling constants (*J*) were given in Hz. Resonance multiplicity was described as s (singlet), d (doublet), t (triplet), m (multiplet) and br (broad signal). Carbon spectra were acquired with a complete decoupling for the proton. High resolution mass spectrometry (HRMS) was performed with a JEOL JMS-700 B/E.

Compound 2: Fuming HNO_3 (14.0 mL, 336 mmol) was added to a solution of **1** (30.0 g, 46.0 mmol) in CH_2Cl_2 (300 mL). The mixture was stirred for 5 h at rt. Subsequently, the solution was cooled in a water-ice bath and Et_3N (45 mL) was added dropwise. The resulting mixture was filtered through a silica plug which was then rinsed with CH_2Cl_2 (300 mL). The solvent was evaporated under reduced pressure and the resulting 1:1 mixture of the 1,6 and 1,7 regioisomers was recrystallized twice (see below) in CH_3CN to yield the regiopure 1,6 regioisomer **2** (11.80 g, 39%) as a red solid. ^{1}H NMR (500 MHz, $CDCl_3$): δ 8.39 (s, 2H), 8.06 (m, 4H), 4.36 (m, 8H), 1.79 (m, 8H), 1.49 (m, 8H), 1.00 (m, 12H). ^{13}C NMR (125 MHz, $CDCl_3$): 167.7, 166.1, 147.7, 133.5, 131.0, 130.9, 130.2, 129.5, 128.8, 128.3, 128.2, 127.2, 127.0, 126.6, 66.6, 66.1, 30.7, 30.6, 19.4, 19.3, 13.9, 13.9. HRMS calcd. for $C_{40}H_{42}N_2O_{12}$ ($[M]^-$): 742.2743 found: 742.2752 (1.13 ppm error).

Typical recrystallization procedure: The solid obtained after nitration was placed in a 1 L flask with a stirring bar before 250 mL of CH_3CN were added. The suspension was vigorously stirred at reflux temperature for 30 min. If the solid was not dissolved in these conditions, more solvent was added progressively by increments of 50 mL. The mixture was allowed to reach the reflux temperature after every new addition before determining if more solvent was necessary. When the solid was completely dissolved (approximatively after 400 or 500 mL of solvent have been used in total), the mixture was allowed to slowly cool down to room

temperature. At this stage, the appearance of orange crystals or needles can be observed. After one hour, the orange solid was separated by Büchner filtration and washed with CH_3CN that was previously cooled down to 0 °C with an ice bath (200 mL). The solid recovered after this first recrystallization contains only a small amount of the 1,7 regioisomer (>10%), which can be completely removed by repeating the exact same procedure a second time.

Compound 1,7-4: A suspension of **6** (347 mg, 0.312 mmol) and $AgNO_2$ (2.40 g, 15.6 mmol) in toluene (7 mL) was refluxed for 3 d in a sealed tube under an argon atmosphere. The solvent was evaporated under reduced pressure and the crude material was purified by column chromatography (SiO_2, petroleum ether/CH_2Cl_2 50:50, then 30:70) to afford **1,7-4** (294 mg, 90%) as a red solid. ^{1}H NMR (500 MHz, $CDCl_3$): δ 8.85 (s, 2H), 8.72 (d, J = 8.1 Hz, 2H), 8.32 (d, J = 8.1 Hz, 2H), 4.14 (d, J = 7.4 Hz, 4H), 1.99 (br, 2H), 1.45 - 1.17 (m, 64H), 0.86 (m, 12H). ^{13}C NMR (125 MHz, $CDCl_3$): δ 162.5, 162.0, 148.5, 132.9, 130.6, 129.8, 128.9, 127.8, 126.6, 125.8, 124.7, 124.6, 45.3, 36.8, 32.1, 32.0, 31.8, 30.2, 29.8, 29.8, 29.7, 29.5, 29.4, 26.6, 22.8, 22.8, 14.3. HRMS calcd. For $C_{64}H_{88}N_4O_8$ ([M]$^-$): 1040.6608 found: 1040.6616 (0.80 ppm error).

Acknowledgements

The authors acknowledge the Université d'Angers and SFR MATRIX for the access to the CARMA platform, Dr. Ingrid Freuze for Mass Spectrometry measurements, Benjamin Siegler for NMR experiments. L. L. B thanks the supercomputer facilities of the Mésocentre de calcul de Franche-Comté. This work received support from the "Etoiles Montantes" funding scheme (A. G., project CURVY, 2021_11614) funded by the PULSAR 2021 program from the Région Pays de la Loire and the Université d'Angers, and the Agence Nationale de la Recherche (A. G., PhotoSynth ANR JCJC 2021, ANR-21-CE06-0015-01).

Conflict of Interests

There are no conflicts to declare.

Data Availability Statement

The data that support the findings of this study are available from the corresponding author upon reasonable request.

Keywords: conjugated materials · organic materials · perylenediimides · regiopure materials · synthetic chemistry

[1] W. Jiang, Z. Wang, *J. Am. Chem. Soc.* **2022**, *144*, 14976–14991.
[2] P. Cheng, X. Zhao, X. Zhan, *Acc. Mater. Res.* **2022**, *3*, 309–318.
[3] A. Nowak-Król, K. Shoyama, M. Stolte, F. Würthner, *Chem. Commun.* **2018**, *54*, 13763–13772.
[4] M. Li, H. Yin, G.-Y. Sun, *Appl. Mater. Today* **2020**, *21*, 100799.
[5] V. Sharma, J. D. B. Koenig, G. C. Welch, *J. Mater. Chem. A* **2021**, *9*, 6775–6789.
[6] Z. Li, D. Yang, X. Zhao, Z. Li, T. Zhang, F. Wu, X. Yang, *RSC Adv.* **2016**, *6*, 101645–101651.
[7] J. Yao, Q. Chen, C. Zhang, Z.-G. Zhang, Y. Li, *SusMat* **2022**, *2*, 243–263.
[8] J. Li, P. Li, M. Fan, X. Zheng, J. Guan, M. Yin, *Angew. Chem. Int. Ed.* **2022**, *61*, e202202532.
[9] F. Würthner, C. R. Saha-Möller, B. Fimmel, S. Ogi, P. Leowanawat, D. Schmidt, *Chem. Rev.* **2016**, *116*, 962–1052.
[10] X. Shang, J. Ahn, J. H. Lee, J. C. Kim, H. Ohtsu, W. Choi, I. Song, S. K. Kwak, J. H. Oh, *ACS Appl. Mater. Interfaces* **2021**, *13*, 12278–12285.
[11] W. Yue, W. Jiang, M. Böckmann, N. L. Doltsinis, Z. Wang, *Chem. Eur. J.* **2014**, *20*, 5209–5213.
[12] J. H. Hurenkamp, W. R. Browne, R. Augulis, A. Pugžlys, P. H. M. van Loosdrecht, J. H. van Esch, B. L. Feringa, *Org. Biomol. Chem.* **2007**, *5*, 3354–3362.
[13] G. Li, Y. Zhao, J. Li, J. Cao, J. Zhu, X. W. Sun, Q. Zhang, *J. Org. Chem.* **2015**, *80*, 196–203.
[14] S. Nakazono, Y. Imazaki, H. Yoo, J. Yang, T. Sasamori, N. Tokitoh, T. Cédric, H. Kageyama, D. Kim, H. Shinokubo, A. Osuka, *Chem. Eur. J.* **2009**, *15*, 7530–7533.
[15] A. H. Endres, M. Schaffroth, F. Paulus, H. Reiss, H. Wadepohl, F. Rominger, R. Krämer, U. H. F. Bunz, *J. Am. Chem. Soc.* **2016**, *138*, 1792–1795.
[16] F. Würthner, V. Stepanenko, Z. Chen, C. R. Saha-Möller, N. Kocher, D. Stalke, *J. Org. Chem.* **2004**, *69*, 7933–7939.
[17] Y. Shi, H. Qian, Y. Li, W. Yue, Z. Wang, *Org. Lett.* **2008**, *10*, 2337–2340.
[18] G. Seybold, G. Wagenblast, *Dyes Pigm.* **1989**, *11*, 303–317.
[19] A. Nowak-Król, F. Würthner, *Org. Chem. Front.* **2019**, *6*, 1272–1318.
[20] Q. Shi, J. Wu, X. Wu, A. Peng, H. Huang, *Chem. Eur. J.* **2020**, *26*, 12510–12522.
[21] L. Chen, C. Li, K. Müllen, *J. Mater. Chem. C* **2014**, *2*, 1938–1956.
[22] P. Rajasingh, R. Cohen, E. Shirman, L. J. W. Shimon, B. Rybtchinski, *J. Org. Chem.* **2007**, *72*, 5973–5979.
[23] S. Sengupta, R. K. Dubey, R. W. M. Hoek, S. P. P. van Eeden, D. D. Gunbaş, F. C. Grozema, E. J. R. Sudhölter, W. F. Jager, *J. Org. Chem.* **2014**, *79*, 6655–6662.
[24] R. K. Dubey, A. Efimov, H. Lemmetyinen, *Chem. Mater.* **2011**, *23*, 778–788.
[25] G. Shao, M. Wu, X. Wang, J. Zhao, X. You, D. Wu, J. Xia, *J. Org. Chem.* **2022**, *87*, 14825–14832.
[26] Y. Liu, Y. Wang, L. Ai, Z. Liu, X. Ouyang, Z. Ge, *Dyes Pigm.* **2015**, *121*, 363–371.
[27] P. Simón Marqués, F. Tintori, J. M. Andrés Castán, P. Josse, C. Dalinot, M. Allain, G. Welch, P. Blanchard, C. Cabanetos, *Sci. Rep.* **2020**, *10*, 3262.
[28] L. Rocard, A. Goujon, P. Hudhomme, *Molecules* **2020**, *25*, 1402.
[29] R. El-Berjawi, P. Hudhomme, *Dyes Pigm.* **2018**, *159*, 551–556.
[30] M. Hruzd, L. Rocard, A. Goujon, M. Allain, T. Cauchy, P. Hudhomme, *Chem. Eur. J.* **2020**, *26*, 15881–15891.
[31] A. Makhloutah, D. Hatych, T. Chartier, L. Rocard, A. Goujon, F.-X. Felpin, P. Hudhomme, *Org. Biomol. Chem.* **2022**, *20*, 362–365.
[32] M. Schulze, M. Philipp, W. Waigel, D. Schmidt, F. Würthner, *J. Org. Chem.* **2016**, *81*, 8394–8405.
[33] M. Schulze, A. Steffen, F. Würthner, *Angew. Chem. Int. Ed.* **2015**, *54*, 1570–1573; *Angew. Chem.* **2015**, *127*, 1590–1593.
[34] L. Hao, W. Jiang, Z. Wang, *Tetrahedron* **2012**, *68*, 9234–9239.
[35] A. Goujon, L. Rocard, H. Melville, T. Cauchy, C. Cabanetos, S. Dabos-Seignon, P. Hudhomme, *J. Mater. Chem. C* **2022**, *10*, 14939–14945.
[36] H. Sun, Z. Mu, C. Yang, K. Zhang, X. Ji, T. Zhang, H. Ding, S. Wang, L. Dong, J. Zhang, Q. Zhang, *Chem. Asian J.* **2022**, *17*, e202101323.
[37] H. Sun, J. Jin, Q. Wang, S. Wang, W. Na, Z. Li, B. Yao, P. Sun, L. Dong, X.-C. Hang, *Dyes Pigm.* **2022**, *200*, 110169.
[38] A. Makhloutah, A. Hoff, A. Goujon, G. C. Welch, P. Hudhomme, *Mater. Chem. Front.* **2022**, *6*, 3237–3242.
[39] H.-Y. Tsai, K.-Y. Chen, *J. Lumin.* **2014**, *149*, 103–111.
[40] K.-Y. Chen, T. J. Chow, *Tetrahedron Lett.* **2010**, *51*, 5959–5963.
[41] H.-Y. Tsai, K.-Y. Chen, *Dyes Pigm.* **2013**, *96*, 319–327.
[42] H.-Y. Tsai, C.-W. Chang, K.-Y. Chen, *Tetrahedron Lett.* **2014**, *55*, 884–888.
[43] K.-Y. Chen, C.-W. Chang, H.-Y. Tsai, *Materials* **2015**, *8*, 4943–4960.
[44] Y. Zhang, Z. Zhao, X. Huang, Y. Xie, C. Liu, J. Li, X. Guan, K. Zhang, C. Cheng, Y. Xiao, *RSC Adv.* **2012**, *2*, 12644.
[45] P. J. Amal Joseph, S. Priyadarshini, M. Lakshmi Kantam, H. Maheswaran, *Tetrahedron Lett.* **2012**, *53*, 1511–1513.
[46] S. Saito, Y. Koizumi, *Tetrahedron Lett.* **2005**, *46*, 4715–4717.

[47] Paik, Seung-Uk, Jung, Myoung-Geun, *Bull. Korean Chem. Soc.* **2012**, *33*, 689–691.
[48] G.-A. Lee, H.-C. Lin, H.-Y. Lee, C.-H. Chen, H.-Y. Huang, *Asian J. Org. Chem.* **2017**, *6*, 1733–1736.
[49] A. Goujon, L. Rocard, T. Cauchy, P. Hudhomme, *J. Org. Chem.* **2020**, *85*, 7218–7224.
[50] C. Mahmoudi, I. Bulut, J. Jing, S. Fall, B. Heinrich, S. Méry, T. Heiser, P. Lévêque, E. Steveler, M. Majdoub, N. Leclerc, *Eur. J. Org. Chem.* **2021**, *2021*, 3170–3177.
[51] A. Can, A. Facchetti, H. Usta, *J. Mater. Chem. C* **2022**, *10*, 8496–8535.
[52] A. Garci, J. A. Weber, R. M. Young, M. Kazem-Rostami, M. Ovalle, Y. Beldjoudi, A. Atilgan, Y. J. Bae, W. Liu, L. O. Jones, C. L. Stern, G. C. Schatz, O. K. Farha, M. R. Wasielewski, J. Fraser Stoddart, *Nat. Catal.* **2022**, *5*, 524–533.
[53] B. Roy, I. Maisuls, J. Zhang, F. C. Niemeyer, F. Rizzo, C. Wölper, C. G. Daniliuc, B. Z. Tang, C. A. Strassert, J. Voskuhl, *Angew. Chem. Int. Ed.* **2022**, *61*, e202111805.
[54] P. Simón Marqués, J. M. Andrés Castán, L. A. Galan, M. Allain, O. Maury, T. Le Bahers, P. Blanchard, C. Cabanetos, *J. Org. Chem.* **2021**, *86*, 5901–5907.
[55] E. P. Farr, M. T. Fontana, C.-C. Zho, P. Wu, Y. L. Li, N. Knutson, Y. Rubin, B. J. Schwartz, *J. Phys. Chem. C* **2019**, *123*, 2127–2138.
[56] D. Aranda, N. J. Schuster, X. Xiao, F. J. Ávila Ferrer, F. Santoro, C. Nuckolls, *J. Phys. Chem. C* **2021**, *125*, 2554–2564.
[57] S. R. Bora, D. J. Kalita, *New J. Chem.* **2022**, *46*, 19357–19372.

Manuscript received: February 28, 2023
Accepted manuscript online: April 11, 2023
Version of record online: April 27, 2023